Journal of Zhejiang University-SCIENCE A (Applied Physics & Engineering)
ISSN 1673-565X (Print); ISSN 1862-1775 (Online)
www.jzus.zju.edu.cn; www.springerlink.com
E-mail: jzus@zju.edu.cn

A model of two cylindrical plane wall layers exposed to oscillating temperatures with different amplitudes and frequencies

Shalom SADIK
(*Department of Mechanical Engineering, Ort Braude College, Karmiel 21982, Israel*)
E-mail: shaloms@braude.ac.il

Received Oct. 3, 2016; Revision accepted May 6, 2017; Crosschecked Nov. 7, 2017

Abstract: A linear model of two cylindrical plane wall layers exposed to oscillating temperatures and frequencies was built using a physical superposition of two states. In the first state, the inner surface of a wall was exposed to oscillating temperature and the outer surface was exposed to a zero relative temperature. In the second state, the inner surface was exposed to a zero relative temperature while the outer surface was exposed to an oscillating temperature with different amplitude and frequency. Temperature distributions were derived for different amplitudes, frequencies, and thermal conductivities. Results show that increasing the frequency decreased the depth of temperature penetration. A high frequency led to extremum temperature values on the surface, while a low frequency allowed gradual temperature changes during the time period. Temperature distribution lines showing simultaneous heat flux entry and exit were not observed.

Key words: Oscillating temperature; Temperature amplitude; Thermal conductivity; Thermal diffusivity
http://dx.doi.org/10.1631/jzus.A1600641 **CLC number:** O551

1 Introduction

Heat transfer into a cylindrical wall is an important issue in some engineering areas. For example, there is a focused effort in investigating the temperature distribution in the cylinder walls of combustion engines. Studies of temperature distribution are needed for predicting the thermal and fatigue stresses produced in the cylinder wall. Fatigue stresses may be produced as a result of boundary temperature oscillations due to the cyclic operation of the engine. Other engineering applications include heat treatment of metals, engine exhaust valves, solid propellant rocket motors, gun tubes, and heat exchangers. Rakopoulos *et al*. (2004a; 2004b) examined the temperature fluctuations in the cylindrical walls of a diesel engine. Based on a theoretical model and experimental measurements, they investigated the penetration of oscillating temperatures into the inner cylinder wall. They showed that increased insulation or a smaller thermal conductivity value led to a larger temperature frequency and a smaller penetration depth. Lu *et al*. (2006) devised a 2D time-dependent analytical solution of a temperature field for any number of cylindrical shells. The analytical solution compared well with a numerical solution. A lumped coefficient representing transient heating of a long cylindrical shell was introduced by Razelos and Lazaridis (1967). One shell surface was under an adiabatic constraint while the other was exposed to oscillating heating. During heating fluctuations, the coefficient remained constant. Sun and Zhang (2015) proposed a finite element solution of a temperature transient response for a cylindrical shell under different heating frequencies at its surfaces. A large temperature gradient and a strong impact were found on the inner surface with the larger heating frequency. A solution of an unsteady 2D temperature field for a cylindrical shell exposed to oscillating temperatures at its surfaces was developed

ORCID: Shalom SADIK, http://orcid.org/0000-0003-4084-493X

by Fazeli *et al*. (2013). They assumed that the shell material was homogeneous and isotropic. They found that by increasing the Bio number the temperature amplitude became less dependent on the dimensionless length, which is the ratio of the outer radius of the cylindrical shell to its length. Jang and Chiu (2007) investigated the temperature field in a hollow cylinder in which step-wise induction heating was performed on the outer surface. They showed that by increasing the air gap the temperature decreased. Barletta and Zanchini (1995) studied the effect of an alternating current on an electric hollow cylindrical resistor. The resistor cavity was empty or filled with a dielectric solid. An analytical solution was found for temperature as a function of length and time. For a large electric current frequency, the temperature distribution in the resistor material and in the dielectric solid became almost uniform. Talaee and Atefi (2011) introduced a non-Fourier solution for a temperature field in a cylindrical shell exposed to an oscillating heat flux. The material shell was assumed to be homogeneous and isotropic. The speed of heat propagation into the material was finite. Keles and Conker (2011) introduced a non-Fourier solution for a transient temperature field in cylindrical and spherical shells. The material shells were assumed to be heterogeneous. They showed that the speed of the thermal wave was reduced as the inhomogeneity parameter values increased. Barletta and Zanchini (1996) produced an analytical solution for a transient temperature distribution with non-uniform heat generation by the Joule effect in a long cylinder. Thermal resonance was found. Talaee *et al.* (2014) devised an analytical solution for the temperature distribution and the associated thermal stresses for a Fourier law and a non-Fourier effect. Using the non-Fourier effect revealed the wavy behavior of the thermal stresses. Daneshjou *et al.* (2015) introduced a solution for the temperature distribution of the heterogeneous material of a cylindrical shell with an unsteady heat source. They found increased temperature variation near the heat source. Chiu and Chen (2002) presented an analytic process for the thermal-stress distribution in an annular fin exposed to an oscillating heat transfer constraint. A larger fin parameter increased the temperature gradient and thermal stresses. Akbarzadeh and Chen (2012) investigated an unsteady temperature distribution in a non-isotropic cylindrical panel. Increasing the non-homogeneity index increased the temperature steady state value. Bas and Keles (2015) presented an analysis of thermal stress distribution in an annular fin exposed to a decreasing time exponent heat flux. The fin temperature increased with time and then decreased after reaching a maximum value. Takabi (2016) introduced a thermal stress distribution based on an analytical and numerical examination of a thick cylindrical shell. The cylindrical shell was made of functionally graded materials (FGMs). The use of FGM caused a reduction in the stress value. Chatterjee *et al.* (2013) presented an unsteady numerical convection examination of a semicircular cylinder exposed to a forced laminar flow. While facing the flow, the heat transfer through the curved surface was larger than the heat transfer through the flat surface. Malekzadeh *et al*. (2012) presented an examination of heat transfer into a functionally graded (FG) cylindrical shell using a non-Fourier effect. They found that the non-Fourier effect could not be neglected for an unsteady heat transfer. Yan and Malen (2013) investigated the efficiency of a thermoelectric power generator (TPG) (A TPG converts heat into electrical power using no moving parts). Efficiency was improved by using an unsteady heat source. Zhang *et al*. (2015) investigated the thermal displacement of a ceramic-metal cylindrical shell. They showed that displacement was very sensitive to material composition. Roslan *et al*. (2014) investigated natural convection associated with an oscillating temperature on a cylinder surface. Heat transfer was increased by increasing the frequency of thermal oscillations.

The aim of this study was to model the temperature distributions of two cylindrical plane wall layers exposed to temperature oscillations of different amplitudes and frequencies. The model was developed using physical superposition and complex numbers.

2 Current model

2.1 General solution

Fig. 1 shows the general problem.

The temperature distribution (T) is a function of the distance coordinate (r) and time (t), i.e., $T(r, t)$. For 1D heat transfer without heat generated, the cylindrical heat diffusion equation is given by

$$\frac{\partial T}{\partial t}=\alpha\frac{1}{r}\frac{\partial}{\partial r}\left(r\frac{\partial T}{\partial r}\right), \tag{1}$$

where α is the thermal diffusivity and is defined as

$$\alpha=\frac{k}{\rho c_{\mathrm{p}}}, \tag{2}$$

where k is the thermal conductivity, ρ is the material density, and c_{p} is the specific heat capacity.

The heat Eq. (1) is transformed into the following configuration:

$$\frac{\partial T}{\partial t}=\alpha\left(\frac{1}{r}\frac{\partial T}{\partial r}+\frac{\partial^2 T}{\partial r^2}\right). \tag{3}$$

Using separation of variables method to solve Eq. (3), the first connection is given by

$$\frac{T'(t)}{T(t)}=\mathrm{i}\omega, \tag{4}$$

where $T'(t)$=dT/dt, ω is the frequency, and i is the imaginary unit. Eq. (4) leads to the time connection:

$$T(t)=d_1\mathrm{e}^{\mathrm{i}\omega t}, \tag{5}$$

where d_1 is the integration coefficient.

The following is the second connection obtained from Eq. (3):

$$r^2T''(r)+rT'(r)-b^2r^2T(r)=0, \tag{6}$$

where $b=\sqrt{\mathrm{i}\omega/\alpha}$. Eq. (6) leads to the coordinate distance connection:

$$T(r)=d_2I_0(br)+d_3K_0(br), \tag{7}$$

where d_2 and d_3 are the differential equation solution coefficients, I_0 is the modified Bessel function of the first kind of zero order, and K_0 is the modified Bessel function of the second kind of zero order.

By defining:

$$c_1=d_1d_2, \tag{8}$$

$$c_2=d_1d_3, \tag{9}$$

the general solution $T(r, t)$ is given by

$$T=c_1\mathrm{e}^{\mathrm{i}\omega t}I_0(br)+c_2\mathrm{e}^{\mathrm{i}\omega t}K_0(br). \tag{10}$$

In dimensionless form, Eq. (10) is given by

$$T^*=c_1\mathrm{e}^{\mathrm{i}\omega^*t^*}I_0(b^*r^*)+c_2\mathrm{e}^{\mathrm{i}\omega^*t^*}K_0(b^*r^*), \tag{11}$$

where an asterisk as a superscript indicates a dimensionless parameter. Most of the following dimensionless parameters may be based on these average values: $T_{0\mathrm{av}}=(T_{01}+T_{02})/2$, $\omega_{\mathrm{av}}=(\omega_1+\omega_2)/2$, $\alpha_{\mathrm{av}}=(\alpha_1+\alpha_2)/2$, $k_{\mathrm{av}}=(k_1+k_2)/2$. The dimensionless parameters appearing in the following sections are defined as: $T_{01}^*=T_{01}/T_{0\mathrm{av}}$, $T_{02}^*=T_{02}/T_{0\mathrm{av}}$, $\omega_1^*=\omega_1/\omega_{\mathrm{av}}$, $\omega_2^*=\omega_2/\omega_{\mathrm{av}}$, $\alpha_1^*=\alpha_1/\alpha_{\mathrm{av}}$, $\alpha_2^*=\alpha_2/\alpha_{\mathrm{av}}$, $k_1^*=k_1/k_{\mathrm{av}}$, $k_2^*=k_2/k_{\mathrm{av}}$, $r_1^*=r_1/r_3$, $r_2^*=r_2/r_3$, $r_3^*=r_3/r_3=1$. T_{01} and T_{02} are the dimensional amplitude constraints on the internal and external surfaces; r_1, r_2, and r_3 are the dimensional internal radius, boundary radius, and external radius; k_1 and k_2 are the dimensional conductivities of the internal shell and external shell, respectively.

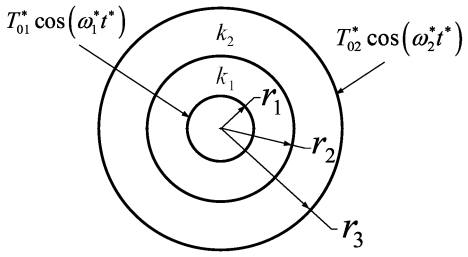

Fig. 1 General problem

2.2 First stage solution

The first stage problem is shown in Fig. 2.

$$T_1^*=c_1\mathrm{e}^{\mathrm{i}\omega_1^*t^*}I_0(b_1^*r^*)+c_2\mathrm{e}^{\mathrm{i}\omega_1^*t^*}K_0(b_1^*r^*), \tag{12}$$

$$T_2^*=c_3\mathrm{e}^{\mathrm{i}\omega_1^*t^*}I_0(b_2^*r^*)+c_4\mathrm{e}^{\mathrm{i}\omega_1^*t^*}K_0(b_2^*r^*), \tag{13}$$

where $b_1^*=\sqrt{\mathrm{i}\omega_1^*/\alpha_1^*}$ and $b_2^*=\sqrt{\mathrm{i}\omega_1^*/\alpha_2^*}$; T_1^* and T_2^* are the dimensionless temperature distributions into

the internal shell and external shell; c_3 and c_4 are the coefficients of the temperature distribution solution into the external shell.

The following connections are the four boundary conditions which are needed to solve the first stage problem:

$$T_1^*\Big|_{r^*=r_1^*} = T_{01}^* \mathrm{e}^{\mathrm{i}\omega_1^* t^*}, \tag{14}$$

$$T_1^*\Big|_{r^*=r_2^*} = T_2^*\Big|_{r^*=r_2^*}, \tag{15}$$

$$k_1^* \frac{\partial T_1^*}{\partial r^*}\bigg|_{r^*=r_2^*} = k_2^* \frac{\partial T_2^*}{\partial r^*}\bigg|_{r^*=r_2^*}, \tag{16}$$

$$T_2^*\Big|_{r^*=r_3^*} = 0. \tag{17}$$

The boundary conditions (Eqs. (14)–(17)) lead to the next algebraic system equations needed to find the temperature distribution coefficients:

$$I_0(b_1^* r_1^*)c_1 + K_0(b_1^* r_1^*)c_2 = T_{01}^*, \tag{18}$$

$$\begin{aligned} &I_0(b_1^* r_2^*)c_1 + K_0(b_1^* r_2^*)c_2 \\ &- I_0(b_2^* r_2^*)c_3 - K_0(b_2^* r_2^*)c_4 = 0, \end{aligned} \tag{19}$$

$$a_1 c_1 - a_2 c_2 - a_3 c_3 + a_4 c_4 = 0, \tag{20}$$

$$I_0(b_2^* r_3^*)c_3 + K_0(b_2^* r_3^*)c_4 = 0, \tag{21}$$

where

$$a_1 = k_1^* b_1^* I_1(b_1^* r_2^*), \tag{22}$$

$$a_2 = k_1^* b_1^* K_1(b_1^* r_2^*), \tag{23}$$

$$a_3 = k_2^* b_2^* I_1(b_2^* r_2^*), \tag{24}$$

$$a_4 = k_2^* b_2^* K_1(b_2^* r_2^*). \tag{25}$$

By defining the following determinants:

$$a_5 = \begin{bmatrix} I_0(b_1^* r_1^*) & K_0(b_1^* r_1^*) & 0 & 0 \\ I_0(b_1^* r_2^*) & K_0(b_1^* r_2^*) & -I_0(b_2^* r_2^*) & -K_0(b_2^* r_2^*) \\ a_1 & -a_2 & -a_3 & a_4 \\ 0 & 0 & I_0(b_2^* r_3^*) & K_0(b_2^* r_3^*) \end{bmatrix}, \tag{26}$$

$$a_6 = \begin{bmatrix} T_{01}^* & K_0(b_1^* r_1^*) & 0 & 0 \\ 0 & K_0(b_1^* r_2^*) & -I_0(b_2^* r_2^*) & -K_0(b_2^* r_2^*) \\ 0 & -a_2 & -a_3 & a_4 \\ 0 & 0 & I_0(b_2^* r_3^*) & K_0(b_2^* r_3^*) \end{bmatrix}, \tag{27}$$

$$a_7 = \begin{bmatrix} I_0(b_1^* r_1^*) & T_{01}^* & 0 & 0 \\ I_0(b_1^* r_2^*) & 0 & -I_0(b_2^* r_2^*) & -K_0(b_2^* r_2^*) \\ a_1 & 0 & -a_3 & a_4 \\ 0 & 0 & I_0(b_2^* r_3^*) & K_0(b_2^* r_3^*) \end{bmatrix}, \tag{28}$$

$$a_8 = \begin{bmatrix} I_0(b_1^* r_1^*) & K_0(b_1^* r_1^*) & T_{01}^* & 0 \\ I_0(b_1^* r_2^*) & K_0(b_1^* r_2^*) & 0 & -K_0(b_2^* r_2^*) \\ a_1 & -a_2 & 0 & a_4 \\ 0 & 0 & 0 & K_0(b_2^* r_3^*) \end{bmatrix}, \tag{29}$$

$$a_9 = \begin{bmatrix} I_0(b_1^* r_1^*) & K_0(b_1^* r_1^*) & 0 & T_{01}^* \\ I_0(b_1^* r_2^*) & K_0(b_1^* r_2^*) & -I_0(b_2^* r_2^*) & 0 \\ a_1 & -a_2 & -a_3 & 0 \\ 0 & 0 & I_0(b_2^* r_3^*) & 0 \end{bmatrix}, \tag{30}$$

the first stage temperature coefficients are given by

$$c_1 = \frac{a_6}{a_5}, \tag{31}$$

$$c_2 = \frac{a_7}{a_5}, \tag{32}$$

$$c_3 = \frac{a_8}{a_5}, \tag{33}$$

$$c_4 = \frac{a_9}{a_5}. \tag{34}$$

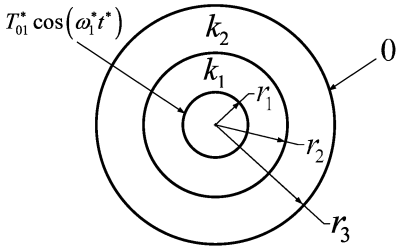

Fig. 2 The first stage problem

2.3 Second stage solution

The second stage problem is shown in Fig. 3.

$$T_{1a}^* = c_{1a} \mathrm{e}^{\mathrm{i}\omega_2^* t^*} I_0(b_3^* r^*) + c_{2a} \mathrm{e}^{\mathrm{i}\omega_2^* t^*} K_0(b_3^* r^*), \tag{35}$$

$$T_{2a}^* = c_{3a} \mathrm{e}^{\mathrm{i}\omega_2^* t^*} I_0(b_4^* r^*) + c_{4a} \mathrm{e}^{\mathrm{i}\omega_2^* t^*} K_0(b_4^* r^*), \tag{36}$$

where $b_3^* = \sqrt{\mathrm{i}\,\omega_2^*/\alpha_1^*}$ and $b_4^* = \sqrt{\mathrm{i}\,\omega_2^*/\alpha_2^*}$, and the

subscript a indicates the second stage.

The following connections are the four boundary conditions which are needed to solve the second stage problem.

$$T_1^*\Big|_{r^*=r_1^*}=0, \tag{37}$$

$$T_1^*\Big|_{r^*=r_2^*}=T_2^*\Big|_{r^*=r_2^*}, \tag{38}$$

$$k_1^*\frac{\partial T_1^*}{\partial r^*}\Big|_{r^*=r_2^*}=k_2^*\frac{\partial T_2^*}{\partial r^*}\Big|_{r^*=r_2^*}, \tag{39}$$

$$T_2^*\Big|_{r^*=r_3^*}=T_{02}^*\mathrm{e}^{\mathrm{i}\omega_2^* t^*}. \tag{40}$$

The boundary conditions (Eqs. (37)–(40)) lead to the next algebraic system equations needed to find the temperature distribution coefficients:

$$I_0(b_3^*r_1^*)c_{1a}+K_0(b_3^*r_1^*)c_{2a}=0, \tag{41}$$

$$\begin{aligned}&I_0(b_3^*r_2^*)c_{1a}+K_0(b_3^*r_2^*)c_{2a}\\&-I_0(b_4^*r_2^*)c_{3a}-K_0(b_4^*r_2^*)c_{4a}=0,\end{aligned} \tag{42}$$

$$a_{1a}c_{1a}-a_{2a}c_{2a}-a_{3a}c_{3a}+a_{4a}c_{4a}=0, \tag{43}$$

$$I_0(b_4^*r_3^*)c_{3a}+K_0(b_4^*r_3^*)c_{4a}=T_{02}^*, \tag{44}$$

where

$$a_{1a}=k_1^*b_3^*I_1(b_3^*r_2^*), \tag{45}$$

$$a_{2a}=k_1^*b_3^*K_1(b_3^*r_2^*), \tag{46}$$

$$a_{3a}=k_2^*b_4^*I_1(b_4^*r_2^*), \tag{47}$$

$$a_{4a}=k_2^*b_4^*K_1(b_4^*r_2^*). \tag{48}$$

By defining the following determinants:

$$a_{5a}=\begin{bmatrix}I_0(b_3^*r_1^*)&K_0(b_3^*r_1^*)&0&0\\I_0(b_3^*r_2^*)&K_0(b_3^*r_2^*)&-I_0(b_4^*r_2^*)&-K_0(b_4^*r_2^*)\\a_{1a}&-a_{2a}&-a_{3a}&a_{4a}\\0&0&I_0(b_4^*r_3^*)&K_0(b_4^*r_3^*)\end{bmatrix}, \tag{49}$$

$$a_{6a}=\begin{bmatrix}0&K_0(b_3^*r_1^*)&0&0\\0&K_0(b_3^*r_2^*)&-I_0(b_4^*r_2^*)&-K_0(b_4^*r_2^*)\\0&-a_{2a}&-a_{3a}&a_{4a}\\T_{02}^*&0&I_0(b_4^*r_3^*)&K_0(b_4^*r_3^*)\end{bmatrix}, \tag{50}$$

$$a_{7a}=\begin{bmatrix}I_0(b_3^*r_1^*)&0&0&0\\I_0(b_3^*r_2^*)&0&-I_0(b_4^*r_2^*)&-K_0(b_4^*r_2^*)\\a_{1a}&0&-a_{3a}&a_{4a}\\0&T_{02}^*&I_0(b_4^*r_3^*)&K_0(b_4^*r_3^*)\end{bmatrix}, \tag{51}$$

$$a_{8a}=\begin{bmatrix}I_0(b_3^*r_1^*)&K_0(b_3^*r_1^*)&0&0\\I_0(b_3^*r_2^*)&K_0(b_3^*r_2^*)&0&-K_0(b_4^*r_2^*)\\a_{1a}&-a_{2a}&0&a_{4a}\\0&0&T_{02}^*&K_0(b_4^*r_3^*)\end{bmatrix}, \tag{52}$$

$$a_{9a}=\begin{bmatrix}I_0(b_3^*r_1^*)&K_0(b_3^*r_1^*)&0&0\\I_0(b_3^*r_2^*)&K_0(b_3^*r_2^*)&-I_0(b_4^*r_2^*)&0\\a_{1a}&-a_{2a}&-a_{3a}&0\\0&0&I_0(b_4^*r_3^*)&T_{02}^*\end{bmatrix}, \tag{53}$$

the second stage temperature coefficients are given by

$$c_{1a}=\frac{a_{6a}}{a_{5a}}, \tag{54}$$

$$c_{2a}=\frac{a_{7a}}{a_{5a}}, \tag{55}$$

$$c_{3a}=\frac{a_{8a}}{a_{5a}}, \tag{56}$$

$$c_{4a}=\frac{a_{9a}}{a_{5a}}. \tag{57}$$

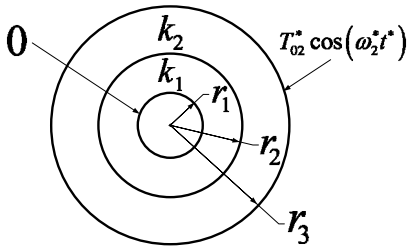

Fig. 3 The second stage problem

2.4 Third stage solution

This stage is a simple superposition of the previous two stages introduced in Sections 2.2 and 2.3.

3 Results and discussion

Fig. 4 introduces five temperature distributions for those same parameters: $\omega_1^*=1$, $\omega_2^*=1$, $\alpha_1^*=$

0.05, $\alpha_2^*=0.01$, $r_1^*=0.3$, $r_2^*=0.6$, $r_3^*=1$, $k_1^*=0.05$, $k_2^*=0.01$. Every case has its specific amplitude relation: for case a, $T_{01}^*=1$, $T_{02}^*=1$; for case b, $T_{01}^*=1$, $T_{02}^*=0.5$; for case c, $T_{01}^*=0.5$, $T_{02}^*=1$; for case d, $T_{01}^*=1$, $T_{02}^*=0$; for case e, $T_{01}^*=0$, $T_{02}^*=1$. Each line in each figure introduced specific time. The time cycle $T_c=2\pi/\omega_{\min}^*$ according to the smaller frequency was divided by 6; thus, each line represents time advance by 1/6 time cycle.

Fig. 5 introduces four temperature distributions for those same parameters: $T_{01}^*=1$, $T_{02}^*=1$, $\alpha_1^*=0.05$, $\alpha_2^*=0.01$, $r_1^*=0.3$, $r_2^*=0.6$, $r_3^*=1$, $k_1^*=0.05$, $k_2^*=0.01$. Every case has its specific frequency relation: for case a, $\omega_1^*=1$, $\omega_2^*=3$; for case b,

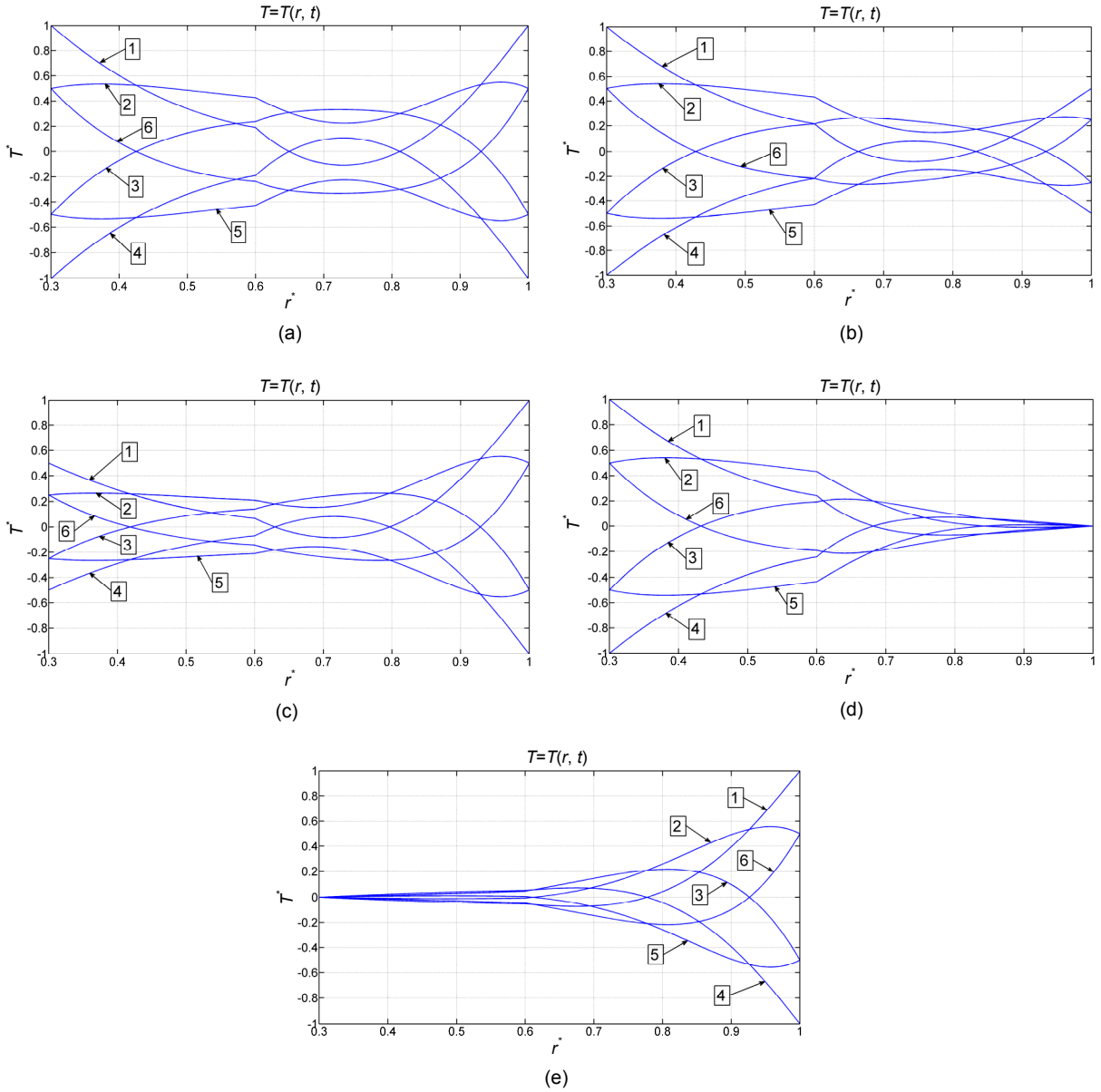

Fig. 4 Five temperature distributions for the parameters listed in Section 2

$\omega_1^*=1$, $\omega_2^*=1$, $\alpha_1^*=0.05$, $\alpha_2^*=0.01$, $r_1^*=0.3$, $r_2^*=0.6$, $r_3^*=1$, $k_1^*=0.05$, $k_2^*=0.01$. The amplitude relations are: (a) $T_{01}^*=1$, $T_{02}^*=1$; (b) $T_{01}^*=1$, $T_{02}^*=0.5$; (c) $T_{01}^*=0.5$, $T_{02}^*=1$; (d) $T_{01}^*=1$, $T_{02}^*=0$; (e) $T_{01}^*=0$, $T_{02}^*=1$

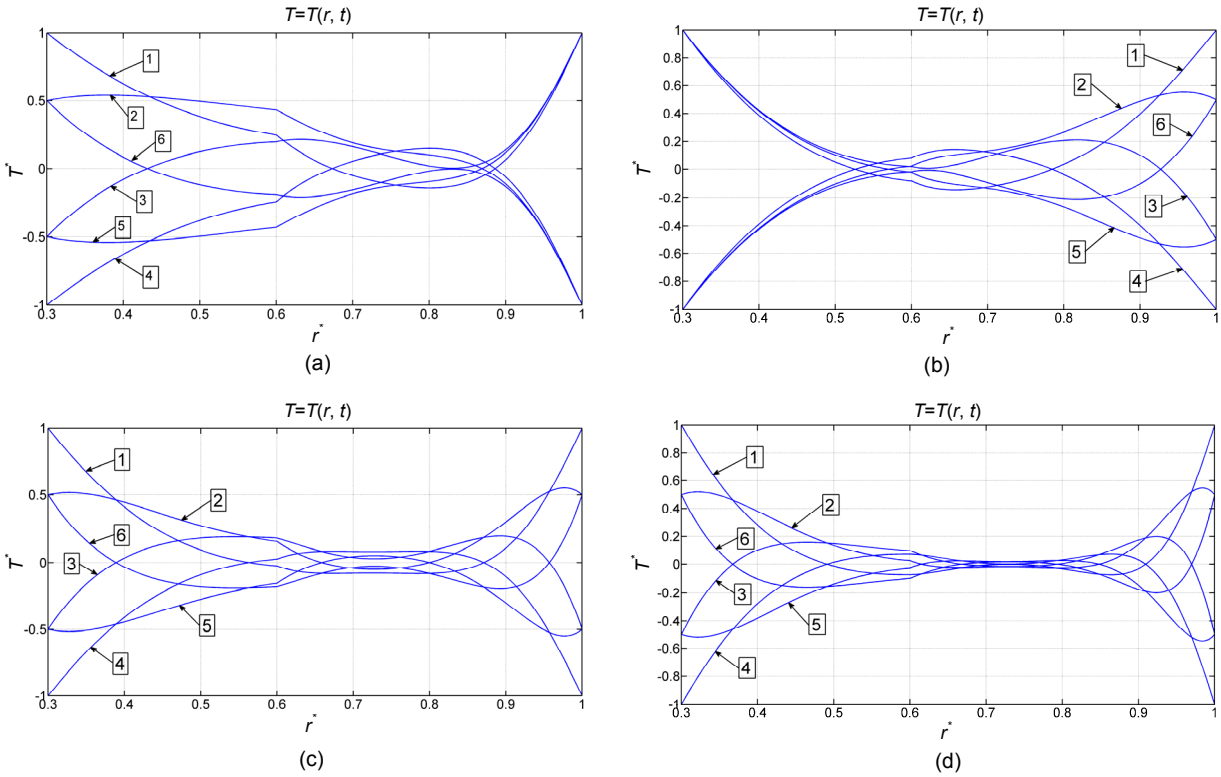

Fig. 5 Four temperature distributions for those parameters listed in Section 2

$T_{01}^*=1$, $T_{02}^*=1$, $\alpha_1^*=0.05$, $\alpha_2^*=0.01$, $r_1^*=0.3$, $r_2^*=0.6$, $r_3^*=1$, $k_1^*=0.05$, $k_2^*=0.01$. The frequency relations are: (a) $\omega_1^*=1$, $\omega_2^*=3$; (b) $\omega_1^*=3$, $\omega_2^*=1$; (c) $\omega_1^*=3$, $\omega_2^*=3$; (d) $\omega_1^*=6$, $\omega_2^*=6$

$\omega_1^*=3$, $\omega_2^*=1$; for case c, $\omega_1^*=3$, $\omega_2^*=3$; for case d, $\omega_1^*=6$, $\omega_2^*=6$.

Fig. 6 introduces three temperature distributions for those same parameters: $T_{01}^*=1$, $T_{02}^*=1$, $\omega_1^*=1$, $\omega_2^*=1$, $r_1^*=0.3$, $r_2^*=0.6$, $r_3^*=1$. Every case has its specific diffusivity and conductivity relations: for case a, $\alpha_1^*=0.01$, $\alpha_2^*=0.05$, $k_1^*=0.01$, $k_2^*=0.05$; for case b, $\alpha_1^*=0.05$, $\alpha_2^*=0.05$, $k_1^*=0.05$, $k_2^*=0.05$; for case c, $\alpha_1^*=0.01$, $\alpha_2^*=0.01$, $k_1^*=0.01$, $k_2^*=0.01$.

Fig. 7 introduces a temperature distribution for the characterized parameters: $T_{01}^*=1$, $T_{02}^*=1$, $\omega_1^*=1$, $\omega_2^*=1$, $\alpha_1^*=0.05$, $\alpha_2^*=0.01$, $k_1^*=0.05$, $k_2^*=0.01$, $r_1^*=0.3$, $r_2^*=0.9$, $r_3^*=1$.

Line 1 in Fig. 4a clearly shows the break point at r^*=0.6 which denotes the boundary surface between the two layers. The line gradient on the left side of the boundary surface is smaller than that on the right. According to the conductivity relations between the two layers $(k_1^*/k_2^*=5)$, a larger gradient results from lower conductivity $(k_2^*=0.05)$. A similar break point is shown for almost all the other lines in Figs. 4 and 5 where the thermal conductivities are not identical. A few more selected examples are line 2 in Fig. 4a, lines 1 and 2 in Fig. 4b, and lines 1 and 2 in Fig. 5a.

Note that the gradient sign does not change while passing through the boundary surface. The above mentioned lines show preservation of negative gradients, while lines 3 and 4 in Fig. 4b, for example, show preservation of positive gradient lines. The amplitude relations are shown clearly in Figs. 4a–4e. The temperature range on the outer surfaces is equal to twice the amplitude of the relevant boundary constraint.

The temperature gradients in Figs. 4–7 show that heat is either entering or leaving through the two surfaces simultaneously: in no case does heat enter

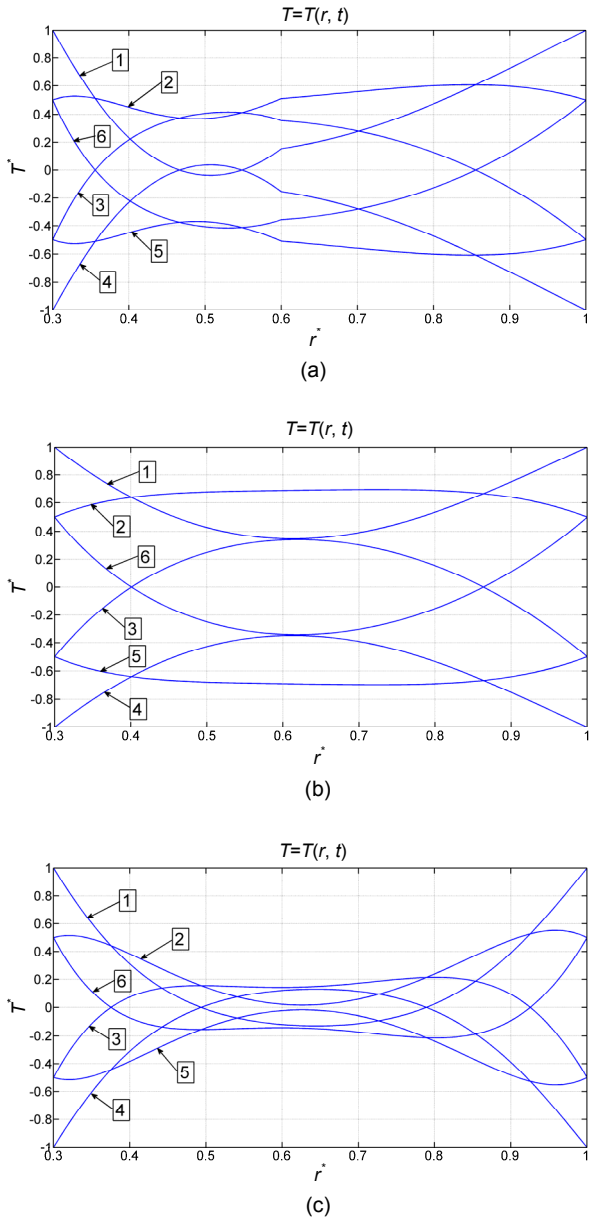

Fig. 6 Three temperature distributions for those parameters listed in Section 2

$T_{01}^*=1$, $T_{02}^*=1$, $\omega_1^*=1$, $\omega_2^*=1$, $r_1^*=0.3$, $r_2^*=0.6$, $r_3^*=1$. The specific diffusivity and conductivity relations are: (a) $\alpha_1^*=0.01$, $\alpha_2^*=0.05$, $k_1^*=0.01$, $k_2^*=0.05$; (b) $\alpha_1^*=0.05$, $\alpha_2^*=0.05$, $k_1^*=0.05$, $k_2^*=0.05$; (c) $\alpha_1^*=0.01$, $\alpha_2^*=0.01$, $k_1^*=0.01$, $k_2^*=0.01$

through one surface and go out through the other at the same time. In Fig. 4a, for example, lines 1 and 2 show heat entering the wall, and lines 2 and 3 show heat leaving simultaneously through the two surfaces. This result may be related to the boundary constraints having the same phase and to the steady positive values of the thermal conductivities.

Figs. 5c ($\omega_1^*=\omega_2^*=3$) and 5d ($\omega_1^*=\omega_2^*=6$) show that increasing the frequency leads to a reduction in the penetration capability of the temperature constraint.

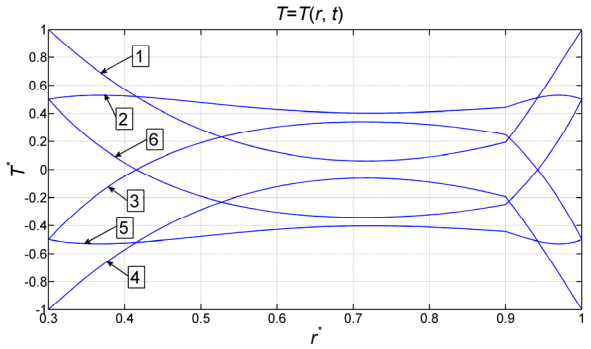

Fig.7 A temperature distribution for the parameters listed in Section 2

$T_{01}^*=1$, $T_{02}^*=1$, $\omega_1^*=1$, $\omega_2^*=1$, $\alpha_1^*=0.05$, $\alpha_2^*=0.01$, $k_1^*=0.05$, $k_2^*=0.01$, $r_1^*=0.3$, $r_2^*=0.9$, $r_3^*=1$

While the constraint frequency at one surface has a large value compared to that at the other surface, as shown in Figs. 5a ($\omega_2^*/\omega_1^*=3$) and 5b ($\omega_1^*/\omega_2^*=3$), the temperature distribution near the higher frequency surface follows the amplitude variation, while the temperature distribution near the lower constraint frequency has values between the amplitude intervals. At a high frequency constraint, the material has difficulty in following the temperature changes. The extremum temperature values are dominant according to the minimum value of the temperature change rate at these points.

Fig. 6a shows the opposite trend of the break point compared to Fig. 4a: the left gradient of all lines in Fig. 6a is larger than that on the right, according to the change in the thermal conductivity values.

A comparison of Figs. 6b and 6c shows that the gradients of the temperature distribution lines with larger conductivity values (Fig. 6b) are lower than those with lower conductivity values (Fig. 6c). Figs. 6b and 6c also show that while the thermal conductivity is uniform, there are no break points in the temperature distribution lines. These results may be considered as a partial validation of the physical model.

The middle surface of the wall is equal to $r^*_{\mathrm{ms}} = 0.3 + 0.7/2 = 0.65$. Fig. 7 shows that the extremum values of the temperature distribution lines are not in the middle of the wall, but in the interval $0.6 < r^*_{\mathrm{ext.}} < 0.65$. Since the middle surface does not divide the cylindrical shell into two equal material quantities (the smaller quantity is near the interior surface), the temperature gradient will be larger near the interior surface and closer to the extremum value.

Fig. 7 shows that the break point of the distribution temperature line moves to r^*=0.9, which is the new separated surface between the two materials or between the two layers.

For constant thermal conductivities and without heat generation the heat diffusion equation mostly leads to a linear connection. Non-linearity potential of the actual physical problem may be due to the use of an improved Fourier law (non-Fourier behavior).

Relevant experimental work is needed to complete the validation of this model.

4 Conclusions

1. Increasing the frequency decreases the depth of temperature penetration.

2. In systems that are working with high frequency and need insulation, it is possible to save material thickness and insulation.

3. Temperature distribution lines showing simultaneous heat flux entry and exit were not found.

4. In contrast to a plane wall, symmetrical constraints will not result in a symmetrical temperature distribution in a cylindrical wall.

5. The temperature distribution more closely tracks the temperature constraints when thermal conductivity is high.

6. The temperature distribution near a high frequency surface constraint follows mostly the constraint extremum values.

7. The use of complex numbers is an appropriate tool to deal with this work and other parallel problems. To build this physical model, a physical superposition has to be used. This work introduces a method that may be used for calculating any number of cylindrical plane walls. This problem has some similarities to a problem comprising fluid layers between oscillating plates, in which the velocity vector takes the place of the scalar temperature value and the kinematic viscosity substitutes for the thermal diffusivity.

References

Akbarzadeh, A.H., Chen, Z.T., 2012. Transient heat conduction in a functionally graded cylindrical panel based on the dual phase lag theory. *International Journal of Thermophysics*, **33**:1100-1125. http://dx.doi.org/10.1007/s10765-012-1204-2

Barletta, A., Zanchini, E., 1995. The temperature field in a cylindrical electric conductor with annular section. *International Journal of Heat and Mass Transfer*, **38**(15): 2821-2832. http://dx.doi.org/10.1016/0017-9310(95)00036-9

Barletta, A., Zanchini, E., 1996. Hyperbolic heat conduction and thermal resonances in a cylindrical solid carrying a steady-periodic electric field. *International Journal of Heat and Mass Transfer*, **39**(6):1307-1315. http://dx.doi.org/10.1016/0017-9310(95)00202-2

Bas, H., Keles, I., 2015. Novel approach to transient thermal stress in an annular fin. *Journal of Thermophysics and Heat Transfer*, **29**(4):705-710. http://dx.doi.org/10.2514/1.T4535

Chatterjee, D., Mondal, B., Halder, P., 2013. Unsteady forced convection heat transfer over a semicircular cylinder at low Reynolds numbers. *Numerical Heat Transfer, Part A: Applications*, **63**:411-429. http://dx.doi.org/10.1080/10407782.2013.742733

Chiu, C., Chen, C., 2002. Thermal stresses in annular fins with temperature-dependent conductivity under periodic boundary condition. *Journal of Thermal Stresses*, **25**(5): 475-492. http://dx.doi.org/10.1080/01495730252890195

Daneshjou, K., Bakhtiari, M., Alibakhshi, R., *et al*., 2015. Transient thermal analysis in 2D orthotropic FG hollow cylinder with heat source. *International Journal of Heat and Mass Transfer*, **89**:977-984. http://dx.doi.org/10.1016/j.ijheatmasstransfer.2015.05.104

Fazeli, H., Abdus, M.A., Karabi, H., *et al*., 2013. Analysis of transient heat conduction in a hollow cylinder using Duhamed theorem. *International Journal of Thermophysics*, **34**(2):350-365. http://dx.doi.org/10.1007/s10765-013-1418-y

Jang, J., Chiu, T., 2007. Numerical and experimental thermal analysis for a metallic hollow cylinder subjected to step-wise electro-magnetic induction heating. *Applied Thermal Engineering*, **27**(11-12):1883-1894. http://dx.doi.org/10.1016/j.applthermaleng.2006.12.025

Keles, I., Conker, C., 2011. Transient hyperbolic heat conduction in thick-walled FGM cylinders and spheres with exponentially-varying properties. *European Journal of Mechanics A/Solids*, **30**(3):449-455. http://dx.doi.org/10.1016/j.euromechsol.2010.12.018

Lu, X., Tervola, P., Viljanen, M., 2006. Transient analytical solution to heat conduction in composite circular cylinder. *International Journal of Heat and Mass Transfer*, **49**(1-2):341-348. http://dx.doi.org/10.1016/j.ijheatmasstransfer.2005.06.019

Malekzadeh, P., Haghighi, M.R., Golbahar, H.Y., 2012. Heat transfer analysis of functionally graded hollow cylinders subjected to an axisymetric moving boundary heat flux. *Numerical Heat Transfer, Part A*, **61**(8):614-632. http://dx.doi.org/10.1080/10407782.2012.670587

Rakopoulos, C.D., Rakopoulos, D.C., Mavropoulos, G.C., *et al*., 2004a. Experimental and theoretical study of the short term response temperature transients in the cylinder walls of a diesel engine at various operating conditions. *Applied Thermal Engineering*, **24**(5-6):679-702. http://dx.doi.org/10.1016/j.applthermaleng.2003.11.002

Rakopoulos, C.D., Antonopoulos, K.A., Rakopoulos, D.C., *et al*., 2004b. Investigation of the temperature oscillations in the cylinder walls of a diesel engine with special reference to the limited cooled case. *International Journal of Energy Research*, **28**:977-1002. http://dx.doi.org/10.1002/er.1008

Razelos, P., Lazaridis, A., 1967. A lumped heat-transfer coefficient for periodically heated hollow cylinders. *International Journal of Heat and Mass Transfer*, **10**(10):1373-1387. http://dx.doi.org/10.1016/0017-9310(67)90027-0

Roslan, R., Saleh, H., Hashim, H., *et al*., 2014. Natural convection in an enclosure containing a sinusoidally heated cylindrical source. *International Journal of Heat and Mass Transfer*, **70**:119-127. http://dx.doi.org/10.1016/j.ijheatmasstransfer.2013.10.011

Sun, Y., Zhang, X., 2015. Transient heat transfer of a hollow cylinder subjected to periodic boundary conditions. *Journal of Pressure Vessel Technology*, **137**:1-10.

Takabi, B., 2016. Thermomechanical transient analysis of a thick-hollow FGM cylinder. *Engineering Solid Mechanics*, **4**:25-32. http://dx.doi.org/10.5267/j.esm.2015.10.002

Talaee, M.R., Atefi, G., 2011. Non-Fourier heat conduction in a finite hollow cylinder with periodic surface heat flux. *Archive of Applied Mechanics*, **81**(12):1793-1806. http://dx.doi.org/10.1007/s00419-011-0518-z

Talaee, M.R., Alizadeh, M., Bakhshandeh, S., 2014. An exact analytical solution of non-Fourier thermal stress in cylindrical shell under periodic boundary condition. *Engineering Solid Mechanics*, **2**(4):293-302. http://dx.doi.org/10.5267/j.esm.2014.8.003

Yan, Y., Malen, J.A., 2013. Periodic heating amplifies the efficiency of thermoelectric energy conversion. *Energy & Environmental Science*, **6**(4):1267-1273. http://dx.doi.org/10.1039/c3ee24158k

Zhang, J., Li, G., Li, S., 2015. Analysis of transient displacements for a ceramic-metal functionally graded cylindrical shell under dynamic thermal loading. *Ceramics International*, **41**(9):12378-12385. http://dx.doi.org/10.1016/j.ceramint.2015.06.070

中文概要

题　目： 不同振幅和频率的振荡温度作用下的双层圆柱壳模型

目　的： 扩大对外表面温度波动约束下的圆柱壳内部温度分布的认识；建立模型并研究同时施加在内外表面的不同振幅和频率的温度波动约束对壳体内温度分布的影响。

创新点： 1. 提出一个清晰的线性模型以获得在外表面施加不同频率和振幅的温度约束时壳体的温度分布；2. 此模型适用于解决导热能力介于理想导热和绝热之间的不同材料组成的任意层数圆柱壳体内的温度分布问题。

方　法： 1. 由热扩散方程和内外表面的边界条件来构建物理模型；2.使用复数和物理叠加以提高该模型的表现。

结　论： 1. 增加表面温度约束的波动频率会相应地减少温度渗透深度；因此，对于高频率工作并需要绝热的系统，可以节约材料厚度并绝热。2. 并未发现同时反映热流的进和出的温度分布线。3. 要构建这个物理模型，必须使用物理叠加。

关键词： 振荡温度；温度振幅；热导率；热扩散率